EPJ E
Soft Matter and Biological Physics
EPJ.org
your physics journal

Eur. Phys. J. E (2015) **38**: 133 DOI 10.1140/epje/i2015-15133-1

Thermodynamic stability in elastic systems: Hard spheres embedded in a finite spherical elastic solid

J.M. Solano-Altamirano and Saul Goldman

edp sciences Società Italiana di Fisica Springer

Eur. Phys. J. E (2015) **38**: 133
DOI 10.1140/epje/i2015-15133-1

THE EUROPEAN PHYSICAL JOURNAL E

Regular Article

Thermodynamic stability in elastic systems: Hard spheres embedded in a finite spherical elastic solid*

J.M. Solano-Altamirano[1,2,a] and Saul Goldman[1]

[1] Department of Chemistry, the Guelph-Waterloo Centre for Graduate Work in Chemistry and the Guelph-Waterloo Physics Institute, University of Guelph, Guelph, Ontario, N1G 2W1, Canada
[2] ELI Beamlines project, Institute of Physics AS CR, v. v. i., Na Slovance 2, 18 221, Prague 8, Czech Republic

Received 6 July 2015 and Received in final form 10 November 2015
Published online: 28 December 2015 –

Abstract. We determined the total system elastic Helmholtz free energy, under the constraints of constant temperature and volume, for systems comprised of one or more perfectly bonded hard spherical inclusions (*i.e.* "hard spheres") embedded in a finite spherical elastic solid. Dirichlet boundary conditions were applied both at the surface(s) of the hard spheres, and at the outer surface of the elastic solid. The boundary conditions at the surface of the spheres were used to describe the rigid displacements of the spheres, relative to their initial location(s) in the unstressed initial state. These displacements, together with the initial positions, provided the final shape of the strained elastic solid. The boundary conditions at the outer surface of the elastic medium were used to ensure constancy of the system volume. We determined the strain and stress tensors numerically, using a method that combines the Neuber-Papkovich spherical harmonic decomposition, the Schwartz alternating method, and Least-squares for determining the spherical harmonic expansion coefficients. The total system elastic Helmholtz free energy was determined by numerically integrating the elastic Helmholtz free energy density over the volume of the elastic solid, either by a quadrature, or a Monte Carlo method, or both. Depending on the initial position of the hard sphere(s) (or equivalently, the shape of the un-deformed stress-free elastic solid), and the displacements, either stationary or non-stationary Helmholtz free energy minima were found. The non-stationary minima, which involved the hard spheres nearly in contact with one another, corresponded to lower Helmholtz free energies, than did the stationary minima, for which the hard spheres were further away from one another.

1 Introduction

The stability of elastic systems is treated in standard texts on elasticity theory [1–4]. The field is old, and its origins can be traced back to Euler [1]. Due to its importance in civil and mechanical engineering, much of the early focus has been on the bending and buckling of columns, beams and plates [1–3]. The stability in these systems, particularly in the earliest work (which pre-dates modern thermodynamics), was usually analyzed on the basis of mechanical stability, specifically, by minimization of the elastic potential energy [1]. In that work, a system was considered stable, when in its minimum mechanical energy configuration. Generally, relatively simple geometries were (and are still) considered, since analytical solutions could be found for them (see for instance [5] for some recent work on the stability of an elastic tube). For more complex systems, numerical methods such as the Finite Element Method, "FEM" (see [6] and references therein), or the Boundary Element Method "BEM" (see [6] and references therein) have been applied. Both methods involve fitting functions to prescribed boundary conditions at the system nodes (which arise from the approximate discretization of the medium's body (FEM), or its boundaries (BEM), in order to solve for the stress and strain tensors in the elastic medium). The solution at an arbitrary point in the medium is found by interpolating the values obtained at the nodes (FEM), or by means of a Green's function integration (BEM) [6]. The computational cost entailed in using FEM or BEM increases with the number of degrees of freedom and this can render complex problems intractable, particularly when hundreds to thousands of initial geometrical configurations need be studied (as in this work). In particular, our problem involves a large number of sub-systems, for each of which, the solution of

* Supplementary material in the form of a pdf file available from the Journal web page at
http://dx.doi.org/10.1140/epje/i2015-15133-1

[a] e-mail: jmsolanoalt@gmail.com

the elastostatic equations is needed. In addition, depending on the method of integration, the stress and strain tensors at a large number of points within the body of the elastic solid need be evaluated, in order to numerically integrate the elastic Helmholtz Free Energy density, over the volume of the elastic solid (below).

As an alternative, for problems involving spherical inclusions such as spheres or spherical cavities, Sadraie *et al.* [7] proposed a method based on combining Neuber-Papkovich-like solutions, the Schwartz alternating method, and Least-squares, for finding the spherical harmonic expansion coefficients that arise in the expressions for distance. We apply this method here because of its ease of implementation and computational efficiency. We also emphasize that here, we do not attempt to explore which is the "best", fastest, or most accurate method, but rather to use one that we consider good enough to be used as a starting point for our purposes. We are interested in getting results for a significant number of initial configurations, and are not primarily concerned with the method to solve the elasticity equations. A key feature that bears on the method's efficiency, is that the number of terms that need be retained in the truncated spherical harmonic expansion does not depend on the number of inclusions, but rather on how close the inclusions get to each other, and to the boundaries of the medium (see [7,8]). Since very close approaches of either kind are not particularly important here, this limitation is essentially irrelevant to the present work. A body of work on thermodynamic stability in elastic systems has been developed over the last half century [9–11], and an excellent, comprehensive, relatively recent treatment, that is available on the internet, was provided by Morris [12].

The purpose of this work is to learn about how shear resistance in a soft elastic solid influences the thermodynamic stability of different shapes that the elastic solid can assume. Our basic motivation stems from our interest in the effect of shear resistance in soft biological tissues (such as kidney tissue), on the preferred state of aggregation of small stones embedded in the tissue. This bears on the problem of the physical basis of solid inclusion agglomeration, which is relevant to whether small stones are induced by elastic forces in their surrounding medium to cluster together to form larger stones. This is obviously important to kidney stone growth. While small inclusions are generally believed to not be problematic, large stones, because of the serious kidney damage and extreme pain they can induce are a major problem in urology [13–15].

The relative contributions of the various mechanisms by which kidney stones grow from a super-saturated solution of calcium salts (mainly calcium oxalate), into large stones are not completely clear. However, there is evidence that kidney stone growth is a multi-step process wherein nucleation and crystal growth (by precipitation of dissolved solutes on to existing nuclei) occur initially. This is believed to be followed by crystal aggregation, and crystal retention [14–16]. While the first two mechanisms are expected to be driven by the degree of super-saturation of the urine with respect to the dissolved salts (which is why kidney stone patients are encouraged to drink lots of water), the aggregation process is more complex and more difficult to study experimentally. Our results will be suggestive of a theoretical basis for crystal coalescence. Specifically, we will find hard particle coalescence to be thermodynamically favoured by elastic shear forces typical of those in soft biological tissues. This is consistent with the observed structure patterns found in kidney stones (see for instance [16]).

Furthermore, there is also a need for a comprehensive theory of thermodynamics of soft solid materials that contain hard embedded inclusions within them. While some preliminary approximate expressions have been derived for the Gibbs Free energy of elastic media containing gas bubbles (in relation to another interest of ours - Decompression Sickness (see [17] and references therein)), the present article, by dealing with a physically simpler type of inclusion (hard immutable spheres) can be more rigorous. As indicated above, we are interested here in whether the shear resistance manifested by an elastic solid acts to separate or to coalesce embedded small hard spheres. Gas bubbles, because they are highly compressible and distortable, present a more complex problem than the one addressed here, and we hope to revisit the more complex gas bubble problem in the future.

Therefore we will focus on finding those geometric configurations of the inclusions (or equivalently, those shapes of the medium) for which the total elastic Helmholtz free energy (HFE) is a minimum. The system will be comprised of a spherically shaped soft elastic solid, with one or more hard spherical inclusions embedded in it. We construct our system by first considering this soft spherical elastic solid, in its initially unstressed and unstrained state. We remove small spheres of this unstressed and unstrained material, and replace the resulting voids with hard spheres, which, by definition, can neither be compressed nor distorted. We will apply Dirichlet boundary conditions to this system as follows. The boundary of the elastic solid at its outer surface will be fixed by a zero displacement vector, which ensures that the deformations of the elastic solid occur at a constant total volume. The spherical hard inclusion(s) will be repeatedly subjected to small rigid displacements from their initial state in an initial stress- and strain-free solid. These displacements create non-zero stresses and strains in the elastic solid, and raise its elastic free energy, relative to its value in the stress- and strain-free state. The medium is taken to be a pure (1-component) material, and the temperature and amount of material in the system will be fixed. Consequently, the total HFE is the appropriate thermodynamic criterion for stability [12]. The total HFE will be determined by numerically integrating the HFE density over the volume of the soft elastic solid.

The calculations are of two kinds. First the strain and stress tensors in the stressed elastic medium containing the embedded inclusions are determined. These are subsequently used to determine the total elastic HFE of the medium. All the calculations are done numerically.

2 Calculations

2.1 Stresses and strains in the elastic medium

2.1.1 Definitions

We will use the word "object" to refer to a cavity, a hard sphere, or a solid elastic sphere, and the inclusions will be taken to be "perfectly bonded". This means that all points in the elastic medium in the un-deformed state are "attached" (in the sense of being mathematically connected) to a point on the surface of the hard inclusion(s), and will remain attached to the corresponding point(s) after the deformation.

2.1.2 The Neuber-Papkovich and Schwarz solutions

The general solution of elastic problems with spherical symmetry has been known for some time. This includes problems such as a spherical cavity embedded in an infinite elastic medium, the solid sphere, the solid elastic shell, and others [18]. The general solution for these problems is known both for Dirichlet and Neumann boundary conditions, which are characterized by prescribed displacements, and prescribed tractions, respectively. The boundary conditions are applied to the concentric spherical surfaces.

The solutions provided by Lur'e [18] are based on the Papkovich-Neuber general solution for problems with spherical symmetry [19,20]. Below, for the sake of completeness in this work, we reproduce these solutions for various types of spherical objects using both Dirichlet and Neumann boundary conditions. These expressions, and their detailed derivations, are given in ref. [18].

Solid sphere, prescribed displacements

When displacements are prescribed at the surface of a spherical solid ($r = r_0$), the solution for the displacement vector at any point in the medium $\boldsymbol{r}$, with $r \leq r_0$, is

$$\boldsymbol{u} = \boldsymbol{U} + \frac{1}{2}\left(r_0^2 - r^2\right)\sum_{n=2}^{\infty}\frac{\nabla\nabla\cdot\boldsymbol{U}_n}{(3-4\nu)+n+2\nu-2}\,. \quad (1)$$

In eq. (1) it is assumed that the prescribed displacements can be written as

$$\boldsymbol{U} = \sum_{n=0}^{\infty}\left(\frac{r}{r_0}\right)^n \boldsymbol{Y}_n^{(\boldsymbol{u})}(\theta,\varphi) \equiv \sum_{n=0}^{\infty}\boldsymbol{U}_n, \quad (2)$$

where $\boldsymbol{Y}_n^{(\boldsymbol{u})}(\theta,\varphi)$ is a vector whose i-th component is

$$\left[\boldsymbol{Y}_n^{(\boldsymbol{u})}(\theta,\varphi)\right]^i \equiv \boldsymbol{Y}_n^{(u_i)}(\theta,\varphi) = \sum_{m=0}^{n} P_n^m(\cos\theta)\left[A_{n,m}^{(u_i)}\cos(m\varphi) + B_{n,m}^{(u_i)}\sin(m\varphi)\right]. \quad (3)$$

The sum on the right of eq. (3) is over the spherical harmonics, $P_n^m(\cos\theta)$ is an associated Legendre polynomial, and (θ,φ) are the polar and azimuthal co-ordinates of a point on the surface of a sphere [21]. Also, in eq. (1), ν is the Poisson ratio of the elastic medium, which is a measure of the amount of transverse stretching or contraction, that results from an applied strain along a particular direction.

Spherical cavity in an infinite elastic medium, prescribed displacements

For the problem of an infinite solid containing a single spherical cavity centred at the origin of the coordinate system, with prescribed displacements at the boundary of the cavity, the solution for the displacement vector at an arbitrary point $\boldsymbol{r}$, with $r \geq r_0$, is given by

$$\boldsymbol{u} = \boldsymbol{U} + \frac{1}{2}\left(r^2 - r_0^2\right)\sum_{n=0}^{\infty}\frac{\nabla\nabla\cdot\boldsymbol{U}_{-n-1}}{(3-4\nu)(n+1)+2-2\nu}\,, \quad (4)$$

where

$$\boldsymbol{U} = \sum_{n=0}^{\infty}\left(\frac{r_0}{r}\right)^{n+1}\boldsymbol{Y}_{-n-1}^{(\boldsymbol{u})}(\theta,\varphi) = \sum_{n=0}^{\infty}\boldsymbol{U}_{-n-1}, \quad (5)$$

and $\boldsymbol{Y}_{-n-1}^{(\boldsymbol{u})}(\theta,\varphi)$ is the vector whose i-th component is

$$\left[\boldsymbol{Y}_{-n-1}^{(\boldsymbol{u})}(\theta,\varphi)\right]^i \equiv Y_{-n-1}^{(u_i)}(\theta,\varphi) = \sum_{m=0}^{n} P_n^m(\cos\theta)\left[A_{-n-1,m}^{(u_i)}\cos(m\varphi) + B_{-n-1,m}^{(u_i)}\sin(m\varphi)\right]. \quad (6)$$

The coefficients of the expansion are formally defined by

$$A_{n,m}^{(T_i)} = \frac{2n+1}{2\pi\lambda_m}\frac{(n-m)!}{(n+m)!} \times \int_0^{2\pi}\mathrm{d}\varphi\int_{-1}^{1}\{T_i(\mu,\varphi)|_{r=R_0} \times P_n^m(\mu)\cos(m\varphi)\mathrm{d}\mu\}\,, \quad (7)$$

and

$$B_{n,m}^{(T_i)} = \frac{2n+1}{2\pi\lambda_m}\frac{(n-m)!}{(n+m)!} \times \int_0^{2\pi}\mathrm{d}\varphi\int_{-1}^{1}\{T_i(\mu,\varphi)|_{r=R_0} \times P_n^m(\mu)\sin(m\varphi)\mathrm{d}\mu\}\,. \quad (8)$$

from which their values can, in principle, be determined. In eqs. (7) and (8), $\mu \equiv \cos\theta$, $\lambda_{m=0} = 2$ and $\lambda_{m\neq 0} = 1$. Similar expressions for other coefficients are found by exchanging $T_i \to u_i$ and $n \to -n-1$ where appropriate.

However, we will not obtain the expansion coefficients by this method, rather we will obtain them from the solution of a linear system of equations that provide Least-squares fits to an over-determined approximate set of

equations (see sect. 2.2.2, below). The reason for not using the defining expressions to evaluate the coefficients is that the terms $T_i(\theta,\varphi)|_{r=r_0}$ change after every iteration, for every object in the composite system (because of the Schwarz "alternating method" that is used (below)). Also, we do not know, in advance, the functional form of $T_i(\theta,\varphi)|_{r=r_0}$, but rather a set of its values at a finite number of points.

2.1.3 Strain and stress tensors

Assuming we know the coefficients of the harmonic expansion for any of the problems listed in the previous section, we can obtain the strain tensor through direct derivatives of the displacement vector

$$u_{ij} = \frac{1}{2}(\partial_i u_j + \partial_j u_i). \tag{9}$$

Also, we assume our elastic material obeys linear stress/strain relationships (or, equivalently, a generalized Hooke's law), so that [3,22]

$$\sigma_{ij} = \frac{1}{2G}\left(u_{ij} + \frac{\nu}{1-2\nu}u_{kk}\delta_{ij}\right). \tag{10}$$

Thus, by differentiating eqs. (1)-(4), and using the results in eq. (10), we can obtain the strain and stress tensor components in the medium for all the problems described by eqs. (1)-(4).

2.1.4 Schwarz alternating method

If more than one object is embedded in the elastic medium, spherical symmetry is lost. As part of the solution of these problems, we will use the "Schwarz alternating method". Basically, this consists of making a first guess at the expansion coefficients, and then refining them iteratively until they stop changing. The method has been used to solve a variety of problems, both for two- and three-dimensional media, when there is more than one object embedded in the elastic medium. Reference [7] provides a list of authors who have used this method. In particular, Sadraie and Crouch used this method to solve the problem of multiple spherical cavities embedded in an infinite elastic medium [7,8].

In this work, we will apply Sadraie *et al.*'s developments described in refs. [7,8], but also extend them in several ways in order to render them applicable our problem. Unlike Sadraie's work that involved spherical cavities in an infinite medium, we will here solve the problem of multiple hard inclusions (hard spheres) embedded in a finite elastic medium. Moreover, in our work, the outermost boundary of the elastic medium will be fixed, and the hard spheres will be made to execute small rigid displacements. Also, we will here provide solutions for all cases described by eqs. (1)-(4), and also the cases developed in ref. [7].

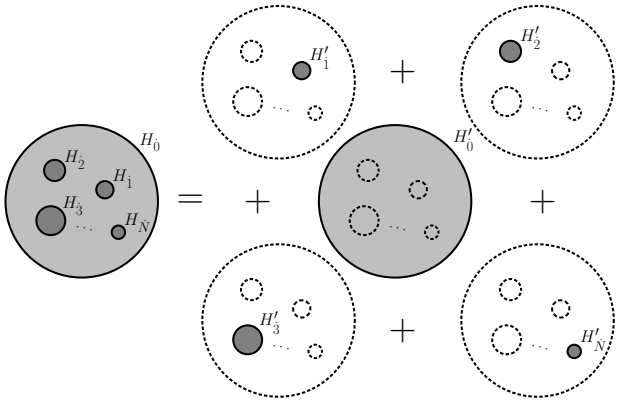

Fig. 1. Decomposition of the actual system of $\dot{N}$ hard spheres embedded in a spherical finite elastic medium (illustrated on the left). The solution (illustrated on the right) is the sum of $\dot{N}+\dot{1}$ superposed solutions of single objects. Each of these objects is subjected to the boundary conditions $H'_{\dot{I}}$, as explained in the text.

2.2 Numerical implementation

As described in Sadraie *et al.* [7,8], when multiple objects are embedded in an elastic medium, the solution can be found with the Schwarz alternating method by superposing harmonic expansions of the form (1), (4), and the respective expressions when tractions are prescribed on the surfaces. For our system, it will be sufficient to use eqs. (1) and (4). For instance, if $\dot{N}$ hard inclusions (we will denote the number of objects by dotted indices) are embedded in an elastic sphere, then the elastic field at any valid point in the elastic spatial domain is found by the sum of superposed objects ($\dot{N}$ hard inclusions and $\dot{1}$ solid elastic sphere), as illustrated in fig. 1.

In the system depicted in fig. 1, the actual system is prescribed the boundary conditions $H_{\dot{I}}$, and the final solution is the sum of that for an isolated system, of the form given by eq. (1) for the elastic medium, and that for $\dot{N}$ isolated systems, whose solution is of the form of eq. (4) for the hard inclusions. Each isolated subsystem is prescribed the boundary conditions $H'_{\dot{I}}$, which are given, after the application of the Schwarz method, by

$$H'_{\dot{I}} = H_{\dot{I}} - \sum_{\dot{I}\neq\dot{J}} H'_{\dot{J}}. \tag{11}$$

Here we use a global Cartesian system of coordinates for the reference coordinate system. For each subsystem (*i.e.* each single object), we translate the global Cartesian coordinates to local Cartesian coordinates. The conversion to local spherical coordinates is done subsequently. This reduces both the computational time and the algebraic complexity that would otherwise have arisen (had we used the addition theorem [23] to translate the spherical coordinates).

In what follows, we will denote as $R_{\dot{I}}$ the collection of all points belonging to each individual boundary of the

```
for ( i=1; i<=NumberOfObjects; i++ ) {
  SetIsolatedCoefficientsToMatchBoundaryConditions();
}
converged=false;
while (converged == false) {
  for ( i=1; i<=NumberOfObjects; i++ ) {
    SetPrescribedDisplacementsToObjectI();
      for ( j=1; j<=NumberOfObjects; j++ ) {
        if ( i != j ) {
          SubtractDisplacementsDueToOtherObjects();
        }
      }
    FitCoefficientsOfObjectIUsingLeastSquareMethod();
    SearchMaximumDifferenceInDisplacementsOfObjectI();
  }
  CheckForConvergence(); //converged = true or false
}
```

Fig. 2. Pseudo-code of the main algorithm for finding the coefficients of the harmonic expansion for all the objects.

$\dot{I}$-th object, *i.e.*

$$R_{\dot{I}} = \left\{ (x,y,z) \,|r_{\dot{I}}^2 = (x-c_{\dot{I}}^x)^2 + (y-c_{\dot{I}}^y)^2 + (z-c_{\dot{I}}^z)^2 \right\}, \tag{12}$$

where $r_{\dot{I}}$ and $\left(c_{\dot{I}}^x, c_{\dot{I}}^y, c_{\dot{I}}^z\right)$ are the radius and the coordinates of the centre of the $\dot{I}$-th object. Quite frequently, we will use the following short-hand notation relative to the centre of the inclusion:

$$d_{\dot{I}} \equiv \sqrt{\left(c_{\dot{I}}^x\right)^2 + \left(c_{\dot{I}}^y\right)^2 + \left(c_{\dot{I}}^z\right)^2}. \tag{13}$$

2.2.1 Main algorithm

To obtain the coefficients of the harmonic expansion of all the objects comprising the system, we use the algorithm depicted in fig. 2. A translation of the algorithm in fig. 2 into English would read as follows. Over-determine the system by setting up more "control points" (points to be fitted) than there are coefficients whose values are sought. Using Least-squares initialize the coefficients to match the system's prescribed boundary condition for each object, as if the object were isolated. Later, within the main loop, apply the prescribed boundary conditions to the set of control points (further described below). For our problem this consists of setting the displacement of every control point located at the surface of an object equal to a constant displacement vector. Then, evaluate the contribution of the remaining objects to the control points, and subtract this from the current object's control points. This is followed by a Least-squares fit to match the updated harmonic expansion coefficients of the current object. Repeat this process for the remaining objects, using the corresponding previously updated coefficients, which were obtained before doing the current object. After this, run a check for convergence to either stop or continue the loop.

Let

$$L_{\dot{I}} = \left\{ (x_{\bar{I}}, y_{\bar{I}}, z_{\bar{I}}) \,|\bar{I} \leq \bar{L},\ \bar{L} \in N^+ \right\} \subset R_{\dot{I}} \tag{14}$$

be the set of control points of the $\dot{I}$-th object, where N^+ denotes positive natural numbers, and let

$$\boldsymbol{u}_{L_{\dot{I}}} \equiv \left\{ \boldsymbol{u}\left(x_{\bar{I}}, y_{\bar{I}}, z_{\bar{I}}\right) | \left(x_{\bar{I}}, y_{\bar{I}}, z_{\bar{I}}\right) \in L_{\dot{I}} \right\} \tag{15}$$

be the set of vector displacements at the points $L_{\dot{I}}$. Let

$$\boldsymbol{u}^0_{L_{\dot{I}}} \equiv \left\{ \boldsymbol{u}^0\left(x_{\bar{I}}, y_{\bar{I}}, z_{\bar{I}}\right) | \left(x_{\bar{I}}, y_{\bar{I}}, z_{\bar{I}}\right) \in L_{\dot{I}} \right\} \tag{16}$$

be the set of prescribed displacement vectors at the control points $L_{\dot{I}}$, and let

$$\boldsymbol{u}^*_{L_{\dot{I}}} \equiv \left\{ \boldsymbol{u}^*_{\bar{I}} \equiv \boldsymbol{u}^*\left(x_{\bar{I}}, y_{\bar{I}}, z_{\bar{I}}\right) | \left(x_{\bar{I}}, y_{\bar{I}}, z_{\bar{I}}\right) \in L_{\dot{I}} \right\} \tag{17}$$

be the set of displacement vectors of the $\dot{I}$-th object at an arbitrary iteration step.

Finally denote

$$\boldsymbol{u}_{\bar{I}}^{j\neq\dot{I}} = \boldsymbol{u}^{j\neq\dot{I}}\left(x_{\bar{I}}, y_{\bar{I}}, z_{\bar{I}}\right) \tag{18}$$

as the displacement vector contribution due to all objects other than $\dot{I}$ at the control point $(x_{\bar{I}}, y_{\bar{I}}, z_{\bar{I}})$. This is the sum of the displacements caused by all the other objects acting on the control points $L_{\dot{I}}$ of the current object.

At each of the iterations, we evaluate the displacement vectors at all control points belonging to each object's boundary as follows:

$$\boldsymbol{u}^*_{L_{\dot{I}}} \supset \boldsymbol{u}^*_{\bar{I}} = \boldsymbol{u}^0_{\bar{I}} - \sum_{j\neq\dot{I}} \boldsymbol{u}^{j\neq\dot{I}}\left(x_{\bar{I}}, y_{\bar{I}}, z_{\bar{I}}\right). \tag{19}$$

Once we have determined the coefficients for the harmonic expansion of each object, *i.e.* after each expansion has met the convergence criteria (below), then we evaluate the displacement vector at any point $\boldsymbol{r}$ as follows:

$$\boldsymbol{u}(\boldsymbol{r}) = \sum_{\dot{I}=\dot{0}}^{\dot{N}} \boldsymbol{u}'_{\dot{I}}\left(\boldsymbol{r}'_{\dot{I}}\right). \tag{20}$$

Here $\boldsymbol{r}'_{\dot{I}}$ is the point $\boldsymbol{r}$ expressed in local coordinates of the $\dot{I}$-th subsystem, and each $\boldsymbol{u}'_{\dot{I}}$ is of the form (1) or (4). The traction vector and the strain and stress tensors are found similarly.

2.2.2 Least-squares method for finding the coefficients of the expansion using control points

Here we describe how we apply Least-squares, through a QR decomposition, to obtain the coefficients of the harmonic expansion of each individual object.

Assuming we truncate the spherical harmonic expansion after the $n = N$ term (see eqs. (1) and (4)), the coefficients $A_{n,m}^{(\boldsymbol{u}_i)}$, $B_{n,m}^{(\boldsymbol{u}_i)}$, $A_{-n-1,m}^{(\boldsymbol{u}_i)}$, and $B_{-n-1,m}^{(\boldsymbol{u}_i)}$ can be arranged into an array "$\mathbf{C}_{\dot{I},n,m}$", designed so that we can

re-write our linear system of equations to have the following structure:

$$\begin{aligned}\mathbf{U}^*_{L_{\dot{I}}} &= \mathbf{M}\left(P_n^m(\mu_{\bar{I}}), \sin(m\varphi_{\bar{I}}), \cos(m\varphi_{\bar{I}})\right)\mathbf{C}_{\dot{I},n,m} \\ &= \mathbf{QRC}_{\dot{I},n,m}. \end{aligned} \tag{21}$$

We use a complete harmonic expansion of N terms for each coordinate x, y, and z. The column vector $\mathbf{U}^*_{L_{\dot{I}}}$ (of $3\bar{L}$ components, or $\bar{L}$ triads) contains all the values of the displacement vectors $\boldsymbol{u}^*_{\bar{I}}$ at every control point of the object (see eq. (19)); $\mathbf{M}(P_n^m(\mu_{\bar{I}}), \sin(m\varphi_{\bar{I}}), \cos(m\varphi_{\bar{I}}))$ is a $3\bar{L} \times (N+1)^2$ matrix which holds the terms $P_n^m(\mu_{\bar{I}}) \cdot \cos(m\varphi_{\bar{I}})$, and $P_n^m(\mu_{\bar{I}}) \cdot \sin(m\varphi_{\bar{I}})$; and $\mathbf{C}_{L_{\dot{I}},n,m}$ is an $(N+1)^2$ array containing the coefficients of the expansion.

Additional technical details will be published elsewhere, and the basic procedure can be found in refs. [7] and [8].

By using the same values for the local coordinates of the control points for each object comprising the system, the QR decomposition needs to be performed only once before entering the main algorithm shown in fig. 2 (see [24]). Subsequently, the $\mathbf{Q}$ and $\mathbf{R}$ matrices can be reused in a back-substitution method to solve the system

$$\mathbf{Q}^{\mathrm{T}}\mathbf{U}^*_{L_{\dot{I}}} = \mathbf{RC}_{\dot{I},n,m}. \tag{22}$$

Here the superscript T means transpose, and a similar procedure is carried out for the coefficients with $n \to -n-1$.

As in refs. [7] and [8], we use an over-determined system of linear equations with $\bar{L} = 4(N+1)^2$. A factor larger than "4" did not improve the accuracy.

The control points are selected from

$$\mu_a = \cos(\theta_a) = 1 - \frac{2(1+a)}{2N+3}, \tag{23}$$

where $a = 0, 1, 2, \ldots, (2N+1)$,

$$\varphi_b = \frac{\pi}{N+1} b, \tag{24}$$

and $b = 0, 1, 2, \ldots, (2N+1)$. Here, θ is the polar angle in the spherical coordinate system, and φ is the azimuthal angle in the x-y plane, *i.e.*, φ is the vector projection angle measured counter-clockwise with respect to the x axis.

Different combinations of the pairs (θ_a, φ_b) are used to construct the set of control points with the barred indices (see eq. (14)). Thus, $\bar{L} = ab = 4(N+1)^2$.

2.2.3 Convergence criteria

As in Sadraie *et al.* [7], at each iteration, and for every object and every control point, we look for the maximum value of the difference between the current value of the displacement vector and its prescribed value, which we denote by $u_{\max}$. Also, in the function FitCoefficientsOfObjectIUsingLeastSquareMethod() in fig. 2, we compare the coefficients of the current and previous iteration for all the objects, and this difference is denoted as $c_{\max}$. The convergence is checked in the function CheckForConvergence(), which is based, essentially, on the following criterion:

$$\begin{aligned}\text{converged} = &\left(|u_{\max}| < \min\left(\delta, \delta|u^0_{\max}|\right)\right) \\ &\&\& \left(|c_{\max}| < \min\left(\eta, \eta|c^0_{\max}|\right)\right). \end{aligned} \tag{25}$$

Here "&&" is the logical operator "AND", $|u^0_{\max}|$ is the analog of $|u_{\max}|$ for the prescribed values (obtained during the initialization in the function SetIsolatedCoefficientsToMatchBoundaryConditions), and $|c^0_{\max}|$ is the equivalent of $|c_{\max}|$ for the initial values of the coefficients. The constants δ and η are two small real numbers which are our tolerances for the displacements and the coefficients, respectively.

Our detailed implementation of the algorithm in fig. 2 differs somewhat from that of Sadraie. This is mainly because we use a global Cartesian coordinate system, and because we find the strain/stress tensor components by differentiating the displacement vectors using a combination of global Cartesian coordinates and local spherical coordinates. However, in order to validate our program, we also solved the problem of two spherical cavities embedded in an infinite elastic medium, with an initial prescribed stress applied at the boundary at infinity. This particular problem has been treated by several authors (see [7] and references therein), and it serves as a benchmark because it contains different methods of solution for the same problem. To an excellent approximation, we were able to obtain the same values for one of the stress tensor components at a set of different prescribed points located on the boundaries of the cavities. The benchmark is valid for different geometric configurations of the cavities (obtained by varying the distance between the cavities' centres). In the supplementary material, we compare our results directly against those obtained by Sadraie *et al.*, and others.

We further verified the accuracy of our calculations by numerically solving the problem of a concentric hollow sphere embedded in a spherical elastic medium, where the inner boundary is given a constant displacement, and the outer boundary is fixed. The analytical solution to this problem is given in ref. [18]. The supplementary material includes comparisons between the analytical solution and the numerical results obtained using our implementation.

Finally, we mention that our program provided the displacement and traction vectors, as well as the stress and strain tensors, at any point in the elastic medium outside of the hard inclusions.

2.3 Elastic free energy

We use Morris' course notes on the thermodynamics of linear elastic solids, to which the reader is referred for further details, and for a very readable and comprehensive treatment of the subject [12]. For reasons of completeness within this work, we also write out some of his relevant results below.

When the characteristic independent variables in the problem are temperature (T), volume (V), numbers of moles of all the components ($\{n\}$), and shape of the system, the Helmholtz free energy F ($= E - TS$, where E and S are the system internal energy and entropy, respectively) is the potential that governs the system. This means, for example, that for a given $T, V, \{n\}$, F will be a minimum when the elastic solid is in its most stable shape.

It is perhaps not superfluous to point out that our system is not isolated. It exchanges both heat and work with the surrounding environment, while being maintained at a constant total volume. Under these conditions the Helmholtz free energy function provides the formally correct criterion for stability. This function will be at a stationary minimum when the system is in its most stable configuration [12,25].

The fundamental variable that unambiguously reflects the shape of the system is the "deviatoric strain tensor", whose elements we designate by u^d_{ij}. These are defined by $u^d_{ij} = u_{ij} - \delta_{ij}u_{kk}/3$, which ensures that the deviatoric strain is a pure shear. The deviatoric strain characterizes the shape of the elastic solid at fixed volume. In terms of its fundamental characteristic variables then, the total system Helmholtz free energy can be written as $F(T, V\{n\}, u^d_{ij})$ [12].

In our problem the deviatoric strain cannot initially be assigned. It is here not a controllable variable, but rather an implicit function of other variables that need to be specified, in order to carry out the calculations for the stress and strain tensors in the final strained state. In order to set up the system, we do the following. First T, $\{n\}$, and the initial volume of the elastic solid V^0 are fixed, such that $u^0_{ij} = \sigma^0_{ij} = 0$ everywhere. Then, the strained elastic solid in the final state is created by a two-step process. 1) We insert exactly fitting hard sphere(s) into pre-existing cavities that had been created at specific locations within the unstrained and unstressed elastic solid. 2) We apply Dirichlet boundary conditions that will both maintain the system at a fixed volume, and create a strained final state with a new shape. The volume is kept fixed by setting the displacement vector at the outer surface of the elastic solid to zero. A non-zero strain throughout the elastic solid, and a change of its shape, is created by displacing the hard sphere inclusion(s) by some small definite amount relative to their initial location. This change is characterized by setting the displacement vector at the surface of the inclusion(s) in the final state to some non-zero value (see also sect. 4.1 and fig. 5 below, for an explicit and graphical explanation). Our calculations ultimately provide the stress and strain tensors throughout the elastic medium, from which the deviatoric strain tensor can be extracted (if desired).

If work against the elastic forces of a solid is done quasi-statically (or, using physical chemistry terminology, "reversibly"), then the total work done in order to achieve a given elastic strain $\boldsymbol{u}$ starting from a strain-free reference state is given by

$$W = \int_V \left(\int_{\mathbf{0}}^{\boldsymbol{u}} \sigma_{ij} \mathrm{d}u_{ij} \right) \mathrm{d}V. \tag{26}$$

The inner integral, which represents the work against elastic forces, per unit volume, is readily carried out by applying Hooke's law, written in generalized form

$$\sigma_{ij} = \sigma^0_{ij} + \lambda_{ijkl} u_{kl}. \tag{27}$$

In eq. (27), σ^0_{ij} is the stress tensor in the strain-free reference state, and λ_{ijkl} is a tensor of the elastic constants that is appropriate to how the strain is accomplished (*e.g.* isothermally, adiabatically, etc.), and is characteristic of the material.

Using eq. (27) for σ_{ij} in eq. (26) gives

$$\begin{aligned} W &= \int_V \left(\int_{\mathbf{0}}^{\boldsymbol{u}} \left[\sigma^0_{ij} + \lambda_{ijkl} u_{kl} \right] \mathrm{d}u_{ij} \right) \mathrm{d}V \\ &= \int_V \left(\sigma^0_{ij} u_{ij} + \frac{1}{2} \lambda_{ijkl} u_{ij} u_{kl} \right) \mathrm{d}V \qquad (28) \\ &= \frac{1}{2} \int_V \left(\sigma^0_{ij} + \sigma_{ij} \right) u_{ij} \mathrm{d}V. \qquad (29) \end{aligned}$$

In going from eq. (28) to eq. (29), we again used Hook's law to replace $\lambda_{ijkl} u_{kl}$ by $(\sigma_{ij} - \sigma^0_{ij})$.

In this work the solid is strained at constant temperature, constant volume, and constant number of moles of material, which is taken to be a pure 1-component elastic solid. Under these conditions, λ_{ijkl} is the tensor of isothermal elastic constants [12], and the work done against the shear resistance of the elastic solid adds directly to the Helmholtz free energy, which can now be written as

$$F\left(T, V, u^d_{ij}\right) = F^0\left(T, V^0\right) + \frac{1}{2} \int_V \left(\sigma^0_{ij} + \sigma_{ij} \right) u_{ij} \mathrm{d}V. \tag{30}$$

In eq. (30) $F^0(T, V^0)$ is the total Helmholtz free energy of the elastic solid in the strain-free reference state at temperature T and volume V^0, and the second term on the right is the elastic strain contribution to the total Helmholtz free energy. Also, since our system is maintained at a fixed volume, $V = V^0$. The term $(\sigma^0_{ij} + \sigma_{ij})u_{ij}/2$ represents the Helmholtz free energy density, *i.e.* the Helmholtz free energy per unit volume, within an infinitesimally small volume element in the elastic medium.

Equation (30) is general, in the sense that it is written to allow for an arbitrary choice of the reference state stress tensor. However, for purposes of carrying out our calculations which require a stress-free reference state [18], we choose the reference state to be stress free. Therefore we set $\sigma^0_{ij} = 0$, so that our working equation for determining the total elastic Helmholtz free energy becomes

$$F^{\mathrm{el}} \equiv (F - F^0) = \frac{1}{2} \int_V \sigma_{ij} u_{ij} \mathrm{d}V. \tag{31}$$

It should be evident from eq. (31), that F^{el} and F will have exactly the same shape-dependence. This is because F^0, the total Helmholtz free energy of the stress- and stain-free reference state, is not shape-dependent. Consequently, the shape corresponding to the minimum F^{el} is the same as

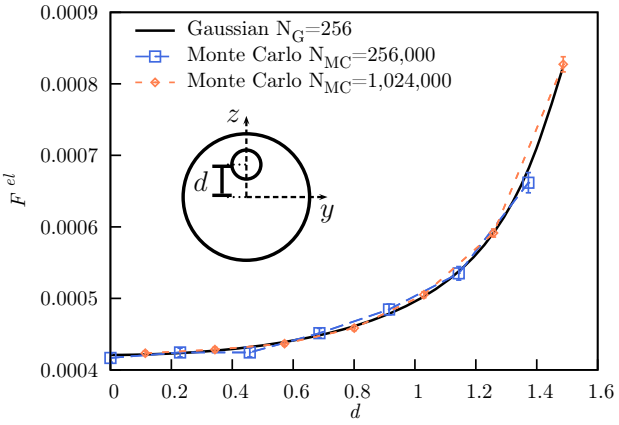

Fig. 3. Comparison of the elastic Helmholtz free energy ($F^{\rm el}$) as a function of the off-centred distance (d) of the inclusion, using different numerical integration schemes. Here $d \equiv d_{\rm i}$ of eq. (13), $F^{\rm el}$ was determined using eq. (31), and $\rm N_G$ and $\rm N_{MC}$ are the numbers of Gauss and Monte Carlo points, respectively.

the shape corresponding to the minimum F, which is the most stable shape the elastic solid can assume.

In what follows, we will use the following definition for the Helmholtz free energy density:

$$f(\boldsymbol{r}) \equiv \frac{1}{2}\sigma_{ij}u_{ij}. \tag{32}$$

3 Overview of computational details

3.1 Accuracy and consistency

The stress and strain tensor components were evaluated as described in sect. 2.1, and their correctness and accuracy were confirmed by checking against the results of other authors, and against some analytical results. Details are provided in Online Resource 1 (see Supplementary Information to this paper).

These components were subsequently used in eq. (31) to determine the total elastic Helmholtz free energy ($F^{\rm el}$). Two numerical schemes were used to evaluate the integral on the right-hand side, which is over the volume of an elastic solid sphere that contains within it one or more embedded hard sphere inclusions at arbitrary locations. The integration domain excludes the embedded spherical inclusions. One was Gauss Quadrature, and the other was a basic Monte Carlo method [21]. The latter, which is robust and easy to apply to irregular geometric domains, was used to check the results from our Gauss Quadrature method, to set error bounds on the calculated free energies, and to handle the case of four embedded hard sphere inclusions, for which the Gauss Quadrature method was impractical.

In fig. 3 we compare the two methods, for the case of a single off-centred inclusion. As seen, the two methods agree to within the Monte Carlo-based error bounds, and the Gauss Quadrature is some 3-4 orders of magnitude faster than the Monte Carlo method. The prescribed displacement vector at the surface of the hard inclusion is here $\boldsymbol{u}_0(R_{\dot{I}}) = (0, 0, 0.1)$, and obviously, changing the sign of the non-zero component produces the same results.

Table 1. Values of the physical parameters used in generating figs. 3 to 11.

Parameter	Symbol	Value (s)
Outer radius of the elastic medium	R_a	2
Radius of the hard inclusion	R_b	0.3
Poisson ratio	σ	0.4996
Shear modulus (atm)	G	0.01
Prescribed displacement magnitude	$\lvert u_0^z \rvert$	0.1

3.2 Computer time requirements

The time to do a single free energy calculation (*i.e.* that for the free energy change resulting from a single displacement of an embedded hard sphere(s)) depended heavily on the numbers of terms retained in the spherical harmonic expansion of the distance (see eqs. (1) and (4), above). We needed to retain 24 to 32 terms for the closest distances we considered. (By a "distance", here, we mean the distance between a hard-sphere boundary and another hard-sphere boundary or to the external boundary of the medium.) A full calculation of the stress and strain tensor components throughout the medium, followed by a numerical integration of the HFE density over the volume of the medium, required from ~ 2 min to ~ 20 min, depending on the numbers of terms retained and on the integration method (for obtaining the HFE), respectively. The calculations were done on a currently standard workstation (quad-core cpu, 2.8 GIG Hz, 16GB RAM).

We point this out in order to provide an indication of what types of calculations were, and were not, feasible. We were able to work out a number of free energy surfaces involving 400 points each, in order to get some idea of the form of the relatively stable hard-sphere configurations (some of them are shown here, and others are given in the Supplementary Information to this paper). However calculation methods designed to seek out and identify the configuration(s) that most likely corresponds to a *global* free energy minimum, such as Simulated Annealing [21], were obviously totally out of the question. Even a fairly modest Simulated Annealing run of 10^6 steps (10 temperatures, each using 10^5 steps), for a point requiring 2 min, would have required about four years to complete on our (standard) workstation.

4 Results

Unless otherwise specified in the figure caption, we used the parameter values entered in table 1 for the figures shown in this and in the previous sections. The values entered for the Poisson ratio and Shear modulus are roughly

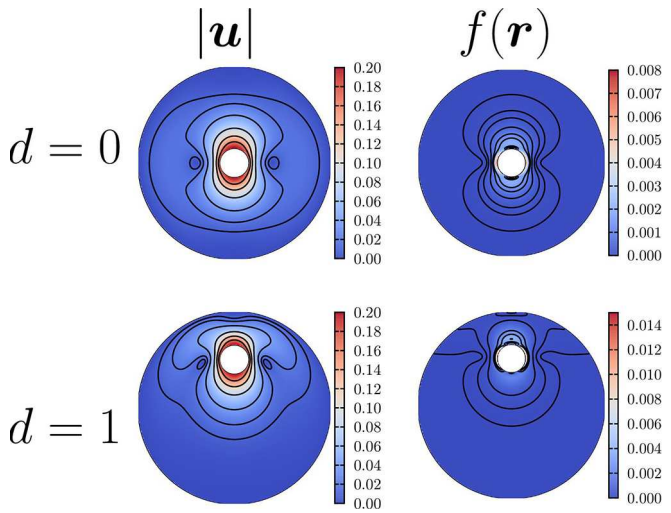

Fig. 4. The magnitude of the displacement vector, and the elastic HFE density for a single hard sphere embedded in an elastic sphere. In the upper row, we show the results for the hard sphere concentric with the medium, and in the lower row we show the results for non-concentric case. Here the radius of the medium is 2, the radius of the inclusion is 0.3, and the magnitude of the prescribed displacement is 0.2.

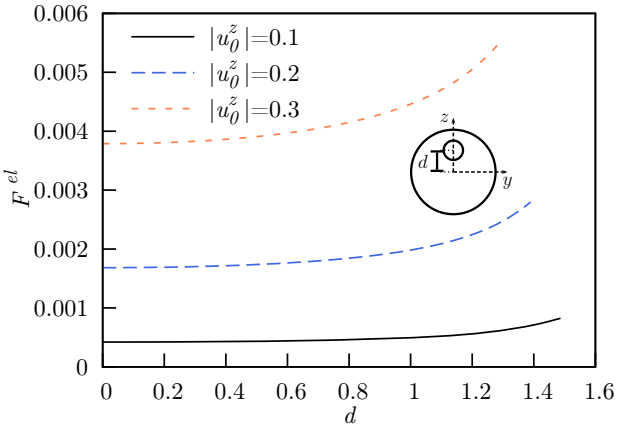

Fig. 5. Elastic Helmholtz free energy ($F^{\rm el}$) as a function of the distance of the inclusion's centre from the origin ("d", measured within the initial stress- and strain-free state), for different values of the magnitude of the displacement vector. The values used for the radius of the hard sphere inclusion and the elastic medium's parameters are entered in table 1.

representative of the values of these functions in soft biological solids such as muscle, liver, heart, cartilage and others [26].

Since a precise assignment of the Poisson ratio and Shear modulus cannot be made for kidney tissue, which is here of particular interest, we include additional results in the Supplementary Information, in order to show the effect of a reasonable variation in the parameter values for these types of materials. Different values of the shear modulus affect the absolute values of the HFE, but not the shape of its landscape.

4.1 One hard inclusion

In fig. 4 we show the elastic HFE density (see eq. (32)), and the magnitude of the displacement vector in the x-z plane of the elastic medium, for two geometric configurations. In the upper and lower rows we show the results for concentric ($d \equiv d_{\rm i} = 0$, see eq. (13)), and non-concentric ($d \neq 0$) geometries, respectively. As expected, the concentric and non-concentric geometries involve respectively, symmetrical and unsymmetrical distributions with respect to the z-axis.

While these plots give the distributions within the x-z plane, the distributions are azimuthally symmetric. In all cases, the prescribed displacement vector for the hard sphere $\boldsymbol{u}_0 = (0, 0, 0.2)$, and it is zero at the outer surface of the elastic medium.

In fig. 5, we illustrate the effect of the magnitude of the displacement vector on the elastic Helmholtz free energy, for a single hard inclusion. We plot the total elastic Helmholtz free energy as a function of distance from the origin of the hard inclusion's centre, for three different values of the displacement vector.

It is worthwhile to briefly pause at this point, and to make explicit the physical meaning of these curves. For definiteness, consider the dashed blue curve. Its point of intersection with the vertical axis (at $d = 0$) is $F^{\rm el} \sim 0.0017$; at $d = 1.4$ its value of $F^{\rm el} \sim 0.0028$. This means that when a hard sphere, initially at $d = 1.4$, of radius 0.3, embedded in an elastic medium of radius 2, shear modulus 0.01, and Poisson ratio 0.4996, is displaced along the z-direction by 0.2 units, with the medium initially stress- and strain-free, the increase in the elastic Helmholtz free energy of the medium is raised by ~ 0.0011 units (*i.e.* $\sim 65\%$) relative to the corresponding increase at $d = 0$. At both the initial and final states of the displacement, the net mechanical force in any direction, exerted on the inclusion by the medium, is exactly zero. This is characteristic of any stable mechanical state in an elastic system, and results from solving the Neuber-Papkovich-like equations for elastic stability. The elastic stresses and strains in the medium re-adjust until the net force on an inclusion, fixed at a particular point, is zero.

Both displacements occur while the total volume of the medium remains constant —a condition ensured by maintaining zero displacement vectors at the outer surface of the medium.

While $F^{\rm el}$ is shown to depend both on the magnitude of the prescribed displacement ($|u_0^z|$), and on "d", a stationary minimum was always found at $d = 0$. Thus, the most stable shape of the elastic medium containing a single inclusion is that of a spherical shell, with the embedded hard sphere —in the stress-free and strain-free medium— at its centre. This result was invariant with the radius of the inclusion, that of the medium, and with the magnitude of the displacement vector (provided the latter is in some sense "small"). This result is a basic manifestation of shear resistance, *i.e.* a tendency to favour the movement of embedded inclusions toward the centre of the material, and away from their outer surface.

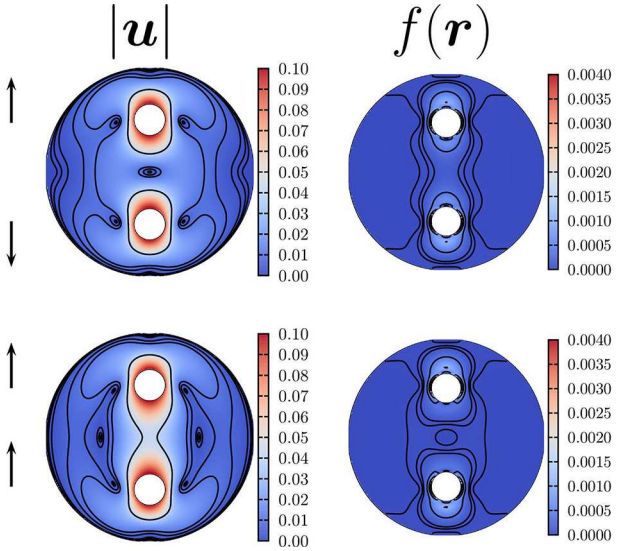

Fig. 6. The magnitude of the displacement vector, and the HFE density for a system with two hard inclusions embedded in an elastic sphere. The upper row shows the case for the hard inclusions given opposite-direction displacements (of the same magnitude), and in the lower row the prescribed displacements are in the same direction for both spheres. The arrows on the left reflect the sign of the u_0^z component of the displacement vector.

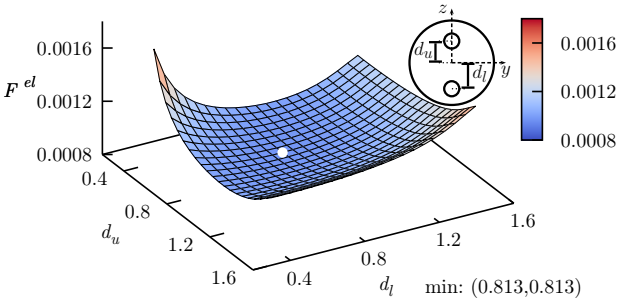

Fig. 7. The total elastic HFE ($F^{\rm el}$) as a function of distances from the origin (d_u, d_l). See also eq. (13) with $d_{\rm i} \to d_u$ and $d_{\rm j} \to d_l$. The two inclusions here have the same radius ($r_u = r_l = 0.3$), and both are subjected to prescribed displacements of the same magnitude (0.1) but in opposite directions (*i.e.*, the hard inclusions approach each other). The white point corresponds to the minimum of the elastic HFE.

4.2 Two hard inclusions

Both the direction and magnitude of the displacement vectors will affect the strain and the HFE density in the medium. In fig. 6, we show the displacement vector's magnitude, and the HFE density (see eq. (32)) in the x-z plane for the hard inclusions undergoing rigid displacements in opposite directions (upper row), and in the same direction (lower row). The displacements have the same magnitude in both cases, and both inclusions have the same radius.

In nature, parallel displacements (that cause inclusion movement in the same direction) will arise more readily than will radial displacements (that cause the inclusions to simultaneously move either towards or away from the centre of the medium). For example, if a person were jumping up and down in a gravitational field, any inclusions present in a soft tissue in their body would be acted upon by a gravitational force simultaneously and in the same direction: down when the person jumps up, and up when the person lands on the ground. Also, sudden horizontal (non-gravitational) accelerations/decelerations of a system would cause non-inertial forces to arise along the direction of motion, and these forces would cause parallel displacements of any hard inclusions.

One the other hand, one requires a laboratory type of environment or set-up to effect radial displacements. This might be imagined to be done by having as inclusions charged conducting spheres of like or unlike signs, where their charge can be turned on or off at will, or spheres made of paramagnetic/diamagnetic materials, with an external magnetic field (which can also be switched on or off at will). This would not occur naturally, but might be done as a test on some of the results shown here.

Here we will consider both types of displacements, and generate a few free energy curves corresponding to each. We do this in order to get some idea of what configurations are favoured by shear resistance, and we will do this both for two inclusions (in this section) and for four inclusions (in sect. 4.3, below).

When both inclusions are displaced in opposite directions (upper row of fig. 6), the elastic system displays small values of the stress and the HFE density in a region near the centre of the medium. The stress is then distributed mostly on the hard inclusions' boundaries which have become closer to the elastic medium's boundary. The plots display the distributions in the x-z plane, but the distributions are azimuthally symmetric. In all cases, the prescribed displacement vectors for the hard inclusions are $\boldsymbol{u}_0 = (0, 0, \pm 0.1)$, and zero for the surface of the elastic medium. The sign of the u_0^z component is a reflection of whether the displacements are proportional to the radius vector of the inclusion centres ($\pm$), or are the same for both inclusions ($+$). (See arrows on the left in fig. 6.)

In figs. 7 and 8 we show the total elastic HFE surfaces, as functions of the upper and lower distances d_u and d_l (defined in the insets).

In fig. 7, both inclusions have the same radius, and the energy landscape is clearly symmetric, with a centred minimum.

In fig. 8 the inclusions have different radii, and the energy surface is no longer symmetric. Here, the larger inclusion tends to be closer to the centre than the smaller inclusion.

In fig. 9, we show the elastic HFE as function of the distances d_u and d_l for the case where both inclusions are subjected to the same displacement (*i.e.* both inclusions are displaced by the same amount, and in the same direction). As seen from the figure, the closer the inclusions are to each other, the lower is the total elastic HFE. In qualitative terms, when the displacements of both inclusions are the same, they behave as though they are parts of a single rigid body.

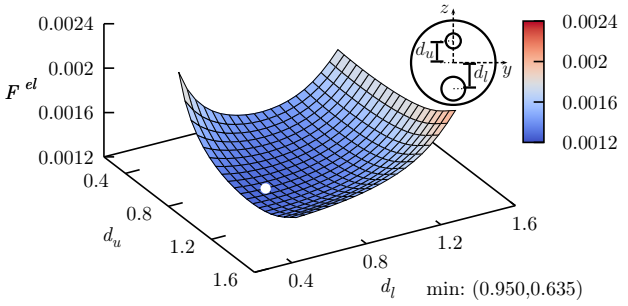

Fig. 8. The total elastic HFE ($F^{\rm el}$) as a function of distances from the origin (d_u, d_l). See also eq. (13) with $d_{\rm i} \to d_u$ and $d_{\dot 2} \to d_l$. The radii of the hard inclusions are $r_u = 0.3$ and $r_l = 0.4$. As in fig. 7, the inclusions are subjected to prescribed displacements of the same magnitude (0.1) but with opposite directions (*i.e.*, the hard inclusions are moving away from each other). The white point corresponds to the minimum of the HFE.

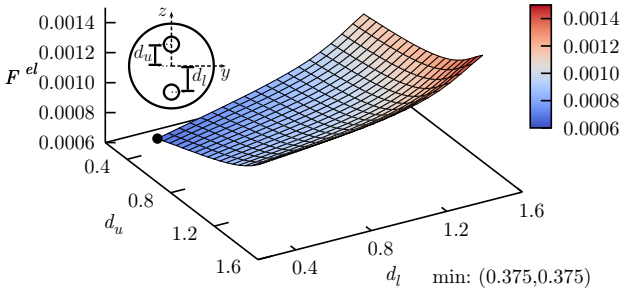

Fig. 9. The elastic HFE ($F^{\rm el}$) as a function of the distances from the origin (d_u, d_l). See eq. (13) with $d_{\rm i} \to d_u$ and $d_{\dot 2} \to d_l$. Here the two inclusions have the same radius ($r_u = r_l = 0.3$) and both are subjected to prescribed displacements of the same magnitude (0.1), in the same direction. The minimum of the elastic HFE (black dot) is located at the lower left corner of the surface. The two hard spheres are here almost in contact with one another.

4.3 More than two inclusions

When more than two inclusions are embedded in the elastic medium, there is no simple way to present the resultant multidimensional elastic total HFE landscape. However, some insight can be gained using specific examples, such as when the inclusions are all located within the same plane, and are all subjected to the same small rigid displacements.

Figure 10 depicts the magnitude of the displacement vector and the elastic HFE density (see eq. (32)) through the plane x-z of an elastic solid system, which contains four inclusions. In the upper row, the inclusions are subjected to small rigid displacements proportional to the radius vector of each inclusion's centre, while in the lower row, the inclusions are subjected to the same small rigid displacement (along the $\hat{k}$ direction). Some rotational symmetry along the y axis is observed for the first case, and the elastic HFE density is higher near the inclusions' boundaries.

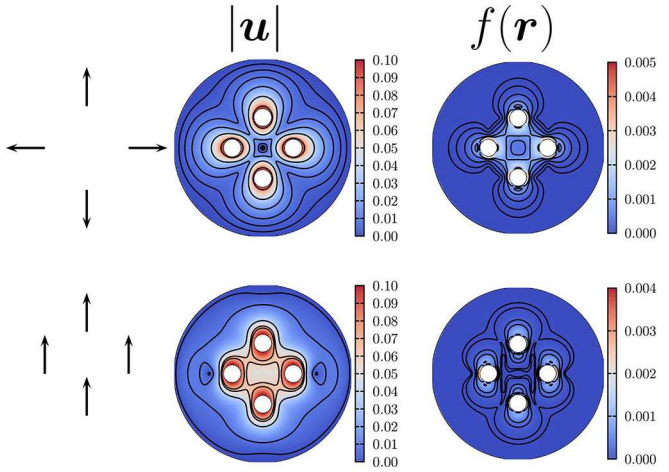

Fig. 10. Distribution of the displacement vector's magnitude and the elastic HFE density for a system with four hard inclusions. The upper row illustrates the case wherein the displacements are proportional to the vector connecting the origin to the centre of the respective hard inclusion. The prescribed displacements here have the same magnitude. In the lower row, we show the case when the prescribed displacements are all in the same direction (here $\hat{k}$). The radius of each inclusion is r_i, and the arrows on the left indicate the direction of the non-zero component of the prescribed displacement.

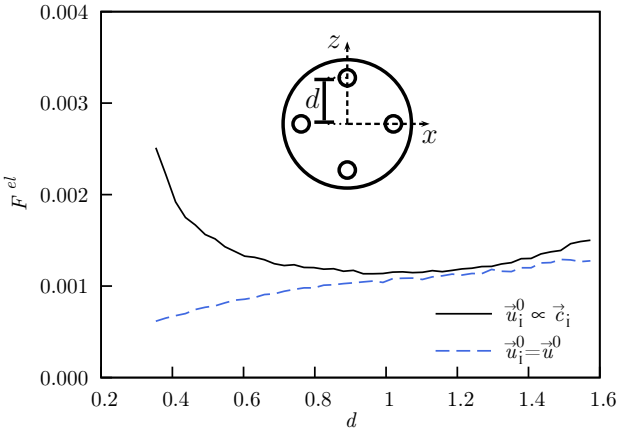

Fig. 11. The total elastic HFE as a function of the distance from the origin d, when the prescribed displacements are proportional to each inclusion's radius vector from the centre (black solid curve), and when the displacements are all taken to be a constant $\boldsymbol{u}_0$ (blue dashed curve). The radius of each inclusion is 0.2, the radius of the elastic medium is 2, and the value of d for each point in the plot is the same for all four hard inclusions. The values of the total elastic HFE were obtained using a Monte Carlo integration for both curves (see text).

In fig. 11 we show the total elastic HFE of a system of four inclusions, as a function of the distance (d) measured from the origin of the elastic medium to the centre of each hard inclusion. For simplicity, all the inclusions in this system are at the same d, and they are all located in the x-z plane. The case wherein the prescribed displacement of each inclusion is radial and proportional to the magnitude of the radius vector of the inclusion's centre, is shown as

the black solid curve, while that for constant prescribed displacements (all in the same direction) are shown by the dashed blue curve.

As with two inclusions (fig. 7), the total elastic HFE has a stationary minimum when d lies somewhere between the elastic medium centre and its boundary (here $d_{\min} \sim 1.1$). In contrast, when the inclusions are subjected to the same prescribed displacement $\boldsymbol{u}_0$ (dashed blue line in fig. 11), a thermodynamic gradient arises, such that the most stable state corresponds to the inclusions being as close as possible to each other ($d \sim 0.35$). This suggests that if the four inclusions were, over time, to be caused to move in parallel, they might escape from their local minimum at $d \sim 1$, $F^{\mathrm{el}} \sim 0.0015$, and form a more stable four-particle near-contact cluster at $d \sim 0.35$, $F^{\mathrm{el}} \sim 0.0005$.

5 Discussion and summary

We found the geometric configurations that present a minimum in the total elastic Helmholtz Free Energy for an elastic solid embedded with one, two, and four perfectly bonded hard sphere inclusions. The elastic medium had a fixed amount of material, and was subjected to constant-volume, constant-temperature deformations. The boundary conditions that provide a constant volume deformation of the elastic solid consist of a zero displacement vector at the outer boundary of the solid, and small displacements of the embedded hard spheres. For systems with more than one embedded hard sphere, we studied two types of displacements: (a) prescribed rigid displacements that are axial and proportional to the vector of the hard sphere centre, and (b) prescribed rigid displacements that have the same constant value for all the hard spheres (*i.e.* the hard spheres are displaced as though they were parts of a single rigid body). For one hard sphere, the most thermodynamically stable state had a stationary elastic Helmholtz free energy minimum, and corresponded to the hard sphere at the centre of the system. For two and four hard spheres, if the prescribed displacements were proportional to the vector of the hard sphere centre, the total elastic HFE had a stationary local minimum located at some distance intermediate between the origin and the boundary of the elastic medium.

For two hard spheres with different radii, the total elastic HFE is a surface with a stable minimum, with the hard spheres separated by some distance. If the system has more than one hard sphere, wherein all are subjected to the same prescribed rigid displacement, then the inclusions have a conditional minimum such that the hard spheres are as close to each other as possible. These conditional minima, for which the hard spheres were nearly in contact, corresponded to lower values of the Elastic HFE than arose using radial displacements, which produced local minima in which the spheres were not in contact. For each type of prescribed displacement, the Helmholtz free energy gradient will, in the long time thermodynamic limit, cause the spheres to favour the configuration corresponding free energy minimum for that type of displacement.

Had the inclusions been *slightly* deformable (as opposed to being perfectly rigid hard spheres), we would expect the HFE landscape to change slightly, but not drastically, or qualitatively. In this case the elastic free energy change of the inclusions would have to be included in the computation of the HFE. But with respect to our motivation, which was to model kidney stones in kidney tissue, we believe that a model of (perfectly rigid) hard spheres in a soft elastic medium is reasonable. Furthermore, provided (as in our work), the total volume of the system remained constant after the displacements, the HFE would again be the criterion for thermodynamic stability.

We are grateful to the Natural Sciences and Engineering Research Council of Canada (NSERC) for financial support in the form of a Discovery Grant (6831-2011) to one of us (SG). JMSA would also like to thank ELI-Beamlines (project CZ.1.05/1.1.00 /02.0061) for providing him the time needed for the final revisions of the paper. We also thank the anonymous reviewers of the *European Physical Journal E*, whose insightful comments helped us to improve the paper. Most of the work for this paper was done at the University of Guelph. JMSA's contribution to the final revision was carried out while he was in the Institute of Physics AS CR.

References

1. A.E.H. Love, *A treatise on the mathematical theory of elasticity*, 2nd edition (Cambridge University Press, 1906).
2. S.P. Timoshenko, J.M. Gere, *Theory of elastic stability*, 2nd edition (McGraw-Hill, 1963).
3. L.D. Landau, E.M. Lifshitz, *Course of Theoretical Physics: Elasticity Theory* (Pergamon Press, 1989).
4. A.S. Saada, *Elasticity: Theory and applications*, 2nd edition (J. Ross Publishing, 2009).
5. M.F. Beatty, J. Elast. **104**, 71 (2011).
6. M. Ameen, *Computational elasticity: theory of elasticity, finite and boundary element methods* (Alpha Science International, 2004).
7. H.R. Sadraie, S.L. Crouch, Comput. Mech. **37**, 60 (2005).
8. H.R. Sadraie, S.L. Crouch, S.G. Mogilevskaya, Eng. Anal. Bound. Elem. **31**, 425 (2007).
9. T.W. Ting, J.C.M. Li, Phys. Rev. **106**, 1165 (1957).
10. T.H.K. Barron, R.W. Munn, Pure Appl. Chem. **22**, 527 (1970).
11. A.G. McLellan, *The classical thermodynamics of deformable materials* (Cambridge University Press, 1980).
12. J.J.W. Morris, Course notes: Thermodynamics and phase transformations, `http://www.mse.berkeley.edu/groups/morris/MSE205/Extras/Elastic.pdf`.
13. A. Mundy, J. Fitzpatrick (Editors), *The Scientific Basis of Urology*, 3rd edition (CRC Press, 2010).
14. J. Baumann, B. Affolter, World J. Nephrol. **3**, 256 (2014).
15. D.R. Basavaraj, C.S. Biyani, A. Browning, J.J. Cartledge, European Association of Urorlogy and European Board of Urology, EAU-EBU Update Series **5**, 126 (2007).
16. A.R. Izatulina, Y.O. Punin, O.A. Golovanova, J. Struct. Chem. **55**, 1225 (2014).
17. S. Goldman, J. Chem. Phys. **132**, 164509 (2010).

18. A.I. Lur'e, D.B. McVean, J.R.M. Radok, *Three dimensional problems of the theory of elasticity* (John Wiley and Sons, Ltd., 1964).
19. P.F. Papkovich, C. R. Acad. Sci. **195**, 513 (1932).
20. H. Neuber, ZAMM-Z Angew. Math. Me. **14**, 203 (1934).
21. W.H. Press, B.P. Flannery, S.A. Teukolski, W. Vetterling, *Numerical Recipes, The art of Scientific Computing (FORTRAN version)* (Cambridge University Press, 1989).
22. S. Timoshenko, J.N. Goodier, *Theory of Elasticity* (McGraw-Hill, 1951).
23. G.B. Arfken, H.J. Weber, *Mathematical methods for physicists*, 6th edition (Elsevier Inc., 2005).
24. I. Jankovic, High-order analytic elements in modeling groundwater flow, Ph.D. thesis, University of Minnesota, Minneapolis (1997).
25. E.A. Guggenheim, *Thermodynamics - An advanced Treatment for Chemists and Physicists* (North-Holland, 1967).
26. J.M. Solano-Altamirano, J.D. Malcolm, S. Goldman, Soft Matter **11**, 202 (2015).